The electronic layer of Mg found in the electron density distribution map obtained by the maximum entropy method

1993 J. Phys.: Condens. Matter 5 8245

(http://iopscience.iop.org/0953-8984/5/44/015)

J. Phys.: Condens. Matter 5 (1993) 8245–8254. Printed in the UK

The electronic layer of Mg found in the electron density distribution map obtained by the maximum entropy method

Y Kubota, M Takata and M Sakata

Department of Applied Physics, Nagoya University, Furo-cho, Chikusa-ku, Nagoya, 464-01, Japan

Received 4 June 1993, in final form 19 August 1993

Abstract. The electron density distribution of HCP (hexagonal close-packed) metal Mg is obtained for the first time by the maximum entropy method (MEM). The data used in the analysis are measured by a newly developed synchrotron x-ray powder diffraction with an imaging plate (IP) as a detector. Care is taken in the quality of the specimen and the high counting statistics of the measurement. In the MEM map of Mg, which is the electron density distribution map obtained by the MEM, a surplus of electron charge is seen around the tetrahedral sites (T sites) of the HCP structure, while the electron densities around the octahedral sites (O sites) are much less than the average density of inter-atomic sites. By these surplus electrons, Mg metal forms a honeycomb network in the basal plane and shows a kind of electronic layer structure. Since there are no ambiguities of phase determination, it can be said that the MEM map of Mg is constructed purely depending on the experimental data and free from any structural models. In our previous work the same kind of honeycomb network was found in Be, which is also an HCP metal. There is a high possibility that such honeycomb network is one of the structural characteristics of pure HCP metals at the electronic level. More work has to be done to investigate such a possibility and the MEM analysis will play an important role in structural studies at the electronic level.

1. Introduction

There are some recent structural studies on HCP metals concerning the anharmonicity of atomic vibration [3–6], but very few about the electron density distributions. Be is the exception. Quite a few studies have been carried out on electron density distributions of Be in order to reveal a bonding nature. The existence of bonding electron around the tetrahedral sites (T sites) was indicated by the Fourier method [7–9]. Yang and Coppens [10] calculated valence and deformation maps and interpreted them to indicate the bonding which they expressed in terms of hybrids of s and p orbitals. They noted that the c/a ratio in Be is smaller than the value for the ideal HCP structure by the bonding due to sp^2 hybrids. In our previous work [2], the electron density distribution of Be was obtained by a newly developed technique of data analysis, namely the maximum entropy method (MEM). The MEM analysis enables one to draw an electron density distribution which is consistent with all the observed structure factors and least biased with respect to the unobserved data without assuming any structural models, which must be very beneficial for experimental studies of the bonding state in Si [11], CeO_2 [12], TiO_2 (rutile) [13], LiF [14] and ice (Ih) [15]. The MEM map of Be showed that the surplus electrons were observed around the T sites, which was consistent with previous results. Furthermore it was revealed for the first time that the surplus electrons around the T sites form the honeycomb networks in the basal plane and show a kind of electronic layer in the Be crystal. Such a feature of bonding could not be found by the conventional Fourier method.

0953-8984/93/448245+10$07.50

Mg is one of the HCP metals of which the c/a value is fairly close to the ideal value. It is noted that the temperature factor for Mg is almost isotropic at room temperature [16]. If any structural anisotropies could be found in Mg, it would be reasonable to expect the same kinds of anisotropy in other HCP metals. Mg has a similar electronic state to that of Be, which has two valence electrons in its atomic s levels in the ground state. It is very interesting to know whether Mg metal forms the same kinds of electronic layer as Be metal. In this work, we measure structure factors of Mg metal by x-ray powder diffraction with high counting statistics and obtain the electron density distribution by the MEM, in order to reveal the bonding nature of Mg metal.

2. Experimental procedure

The MEM map is constructed without any structural models so as to be consistent with the observed data within error bars as a whole. If the data set used in the MEM analysis includes incorrect data, the resultant MEM map will be deformed in various ways, because the resultant MEM map will agree with the incorrect data. It is, therefore, very important to collect accurate data for MEM analysis. X-ray powder diffraction has been employed for the MEM analysis of CeO_2 [12] and TiO_2 (rutile) [13]. The reason is that as long as a good specimen is used in the powder experiment there would be less risk in a powder diffraction experiment for any artificial biases to be introduced than in a single-crystal experiment, which often has a very complicated extinction problem.

For the data collection for Mg, of which the absorption is relatively small, a transmission geometry of powder diffraction was employed. In a transmission geometry, it is not easy to have good counting statistics because of the tiny amount of specimen. For this reason, a new x-ray powder diffraction method [1] which utilizes synchrotron radiation and an imaging plate (IP) as incident x-ray and detector, respectively, was adopted to collect the data. This method is advantageous for crystals composed of only light elements. The powder sample was mounted in a thin-walled silica glass capillary of 0.3 mm diameter. The experiment was carried out by the use of a large Debye–Scherrer camera of 572 mm radius at the Photon Factory BL-$6A_2$. The resolution in angle 2θ was typically about 0.05° full width at half maximum (FWHM). The wavelength of an incident x-ray was 1.04 Å. In order to obtain an x-ray powder pattern with good counting statistics, the exposure time was 4 h, which is very long for an experiment using an IP as a detector. The 20 lowest-angle Bragg reflections with $\sin\theta/\lambda \leqslant 0.54$ Å^{-1} were measured.

3. Profile fitting

The detailed procedure of the whole data analysis, which includes the profile fitting, the scaling and the MEM analysis, is given in [12] and [13]. Here the results of profile fitting will be given briefly.

No extra peaks of oxides were seen in the whole powder pattern. The particle size distribution of the specimen was examined in ω scan data, which are the plots along the Debye–Scherrer line and are sometimes called an ε scan [17]. By the ω scan profile the specimens were considered to be suitable for the collection of accurate Bragg intensities.

The integrated intensities for each Bragg reflection were derived from the x-ray powder pattern by the profile fitting technique. This was carried out by the computer program for profile fitting PRO-FIT [18]. Both split Pearson VII and pseudo-Voigt functions were examined as profile functions and the former was employed in the present analysis because of slightly better fittings for the intensities observed. The results of the profile analysis

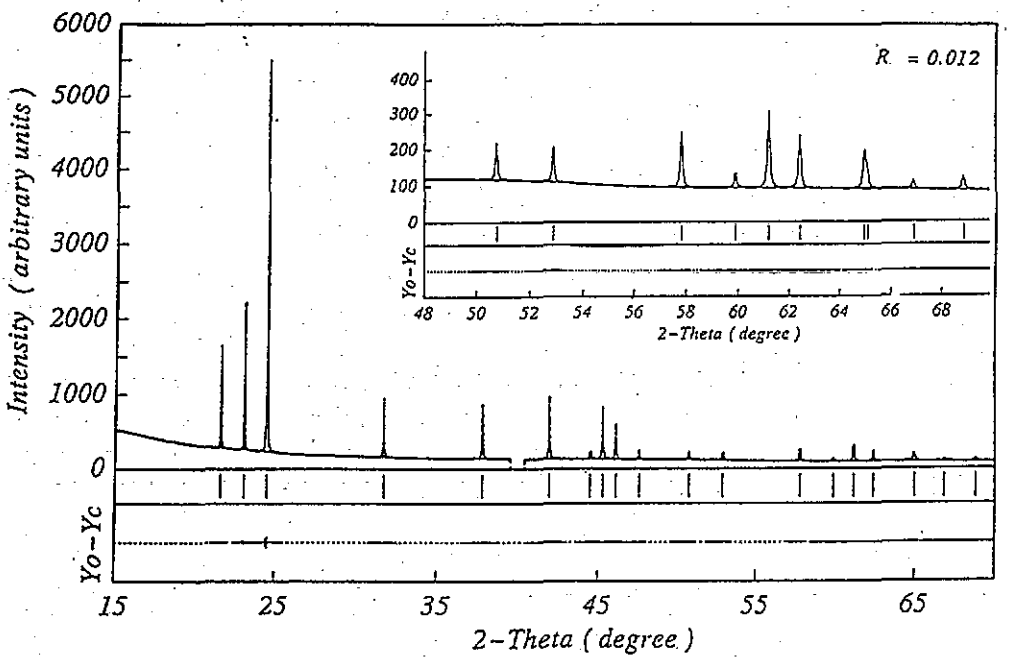

Figure 1. The whole powder pattern of Mg. The observed intensities are collected by transmission powder diffraction in which synchrotron radiation is used as incident x-ray photons and an IP is used as a detector system. The values calculated by profile fitting and the differences between the observed and calculated intensities are also shown.

for Mg are given in figure 1 for the whole powder pattern. In figure 2, typical results of profile fitting are given in detail. The agreements of calculated and observed intensities are very good in both cases. This shows that the individual integrated intensity for each Bragg reflection was estimated in a reasonable way even in the peak overlapped case except for the very severely overlapped peak of (105) and (212) reflections for which the combined intensity was used for further analysis. The combined structure factor is defined as

$$G_{\mathrm{calc}}(j) = \left(\sum_{k'} m_{k'} \mid F_{\mathrm{calc}}(k') \mid^2 \Big/ \sum_{k'} m_{k'} \right)^{1/2}. \tag{1}$$

The definitions of the symbols used in equation (1) are given in Appendix. In general the R values of profile fitting are less than 2% ($R = [\sum w(I_{\mathrm{obs}} - I_{\mathrm{calc}})^2 / \sum w I_{\mathrm{obs}}{}^2]^{1/2}$, $w = I_{\mathrm{obs}}{}^{-1}$) and show good agreements with the observed profiles. The standard deviation of each integrated intensity was estimated by the profile fitting.

In the present analysis, the absorption correction was neglected for the following reason. Considering the low packing ratio of the Mg powder specimen and the short wavelength of incident x-rays, the absorption correction must be quite small. By using the absorption correction formula for a cylindrical sample, the difference of absorption correction factors among the observed reflections was estimated to be at most 0.5%, which should be insignificant compared with the accuracy level of the present intensity measurement.

The scale factor necessary to convert the Bragg integrated intensities to the structure factors was determined by a non-linear least-squares analysis program similar to the POWLS program [19]. The phases of each structure factor were assigned as HCP structure. There must be no possibility that the phases could be misassigned in this way.

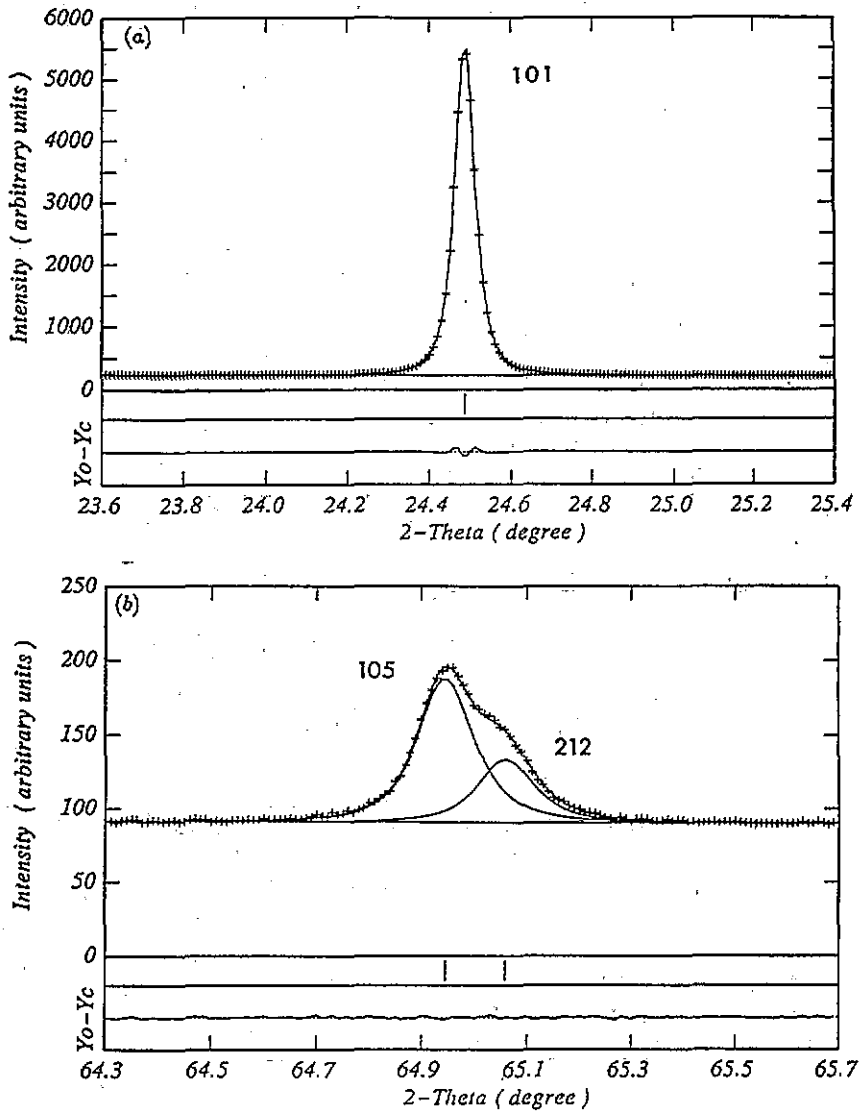

Figure 2. The results of profile fitting (*a*) for a non-overlapped peak of (101) and (*b*) for an overlapped peak of (105) and (212) Bragg reflections of Mg.

Eventually 18 independent structure factors and one combined structure factor were obtained from the integrated intensities, which are both tabulated in table 1. The combined structure factor was calculated from the combined intensity. The effects of preferred orientation were slightly recognized. This effects were considered at the stage of the MEM analysis, which will be shown in the next section.

4. The MEM analysis

Following Collins' approach [20], we have analysed x-ray diffraction data by the MEM in our previous works. Sakata *et al* [13] pointed out that the same MEM equation as Collins' could be derived without using any approximations in the derivation of the MEM equation.

Table 1. The observed integrated intensities, the observed structure factors, the calculated structure factors in which the preferred orientation effects are considered, and the calculated structure factors from the final MEM map of Mg. (105) and (212) reflections are treated as a combined data.

h	k	l	I_{obs}	F_{obs}	F'_{calc}	F_{calc}
1	0	0	188.2(5)	8.4(1)	− 8.4	− 8.8
0	0	2	241(1)	17.4(2)	−17.3	−17.3
1	0	1	802(2)	13.8(2)	−13.2	−13.5
1	0	2	139.3(5)	7.4(1)	7.4	7.4
1	1	0	149.1(5)	12.6(2)	12.5	13.1
1	0	3	173(1)	10.4(1)	10.4	10.4
2	0	0	21.1(3)	5.4(1)	− 5.5	− 5.8
1	1	2	166.0(5)	11.0(1)	−11.0	−11.2
2	0	1	112.0(4)	9.1(1)	9.2	9.5
0	0	4	23.5(2)	10.5(1)	10.6	10.6
2	0	2	26.0(2)	4.8(1)	4.8	4.9
1	0	4	23.0(2)	4.7(1)	− 4.7	− 4.7
2	0	3	43.7(3)	6.9(1)	− 7.0	− 7.1
2	1	0	11.6(3)	3.7(1)	− 3.7	− 3.9
2	1	1	68.0(4)	6.4(1)	− 6.4	− 6.6
1	1	4	44.4(3)	7.4(1)	7.3	7.4
1	0	5	45.4(5)	4.4(1)	4.2	− 6.1
2	1	2				3.4
2	0	4	7.5(3)	3.2(1)	− 3.2	− 3.2
3	0	0	12.8(4)	6.0(1)	6.0	6.2

Hence it was shown that the MEM equation originally derived by Collins can be regarded as rigorous. In order to solve the MEM equation, the zeroth-order single-pixel approximation (ZSPA) is used. Kumazawa *et al* [21] showed that the introduction of ZSPA shall not cause any harm to have the MEM maps.

Using the structure factor data shown in table 1, the MEM map of Mg was iteratively calculated starting from the uniform density by the MEM equation

$$\rho(\boldsymbol{r}) = \exp\left\{\ln\tau(\boldsymbol{r}) + \frac{\lambda F_0}{(N_1+N_2)}\left[\sum_{\boldsymbol{k}}\left[\sigma_F^2(\boldsymbol{k})\right]^{-1}\left[F_{calc}(\boldsymbol{k}) - F_{obs}(\boldsymbol{k})\right]\exp(-2\pi i\boldsymbol{r}\cdot\boldsymbol{k})\right.\right.$$
$$+\sum_j\left(\sigma_G^2(j)G_{calc}(j)\sum_{\boldsymbol{k}'}m_{\boldsymbol{k}'}\right)^{-1}\left[G_{calc}(j) - G_{obs}(j)\right]$$
$$\left.\left.\times\sum_{\boldsymbol{k}'}m_{\boldsymbol{k}'}F_{calc}(\boldsymbol{k}')\exp(-2\pi i\boldsymbol{r}\cdot\boldsymbol{k}')\right]\right\} \tag{2}$$

where

$$F_{calc}(\boldsymbol{k}) = V\sum_{\boldsymbol{r}}\tau(\boldsymbol{r})\exp(-2\pi i\boldsymbol{r}\cdot\boldsymbol{k}). \tag{3}$$

The definitions of the symbols in these equations are also given in Appendix. For the MEM analysis of Mg, the preferred orientation factor for plate like crystals [22]

$$P(\boldsymbol{k}) = \exp\left[-p\,\phi^2(\boldsymbol{k})\right] \tag{4}$$

was used. In order to take into account the preferred orientation effects, the MEM equation, equation (2), is modified by replacing equation (3) with

$$F'_{calc}(\boldsymbol{k}) = F_{calc}(\boldsymbol{k})\,P(\boldsymbol{k})^{1/2}. \tag{5}$$

As a consequence, we have

$$\rho(\boldsymbol{r}) = \exp\Bigg\{\ln\tau(\boldsymbol{r}) + [\lambda F_0/(N_1+N_2)]\Bigg[\sum_{\boldsymbol{k}}\left[\sigma_F^2(\boldsymbol{k})\right]^{-1}\left[F'_{\rm calc}(\boldsymbol{k}) - F_{\rm obs}(\boldsymbol{k})\right]P(\boldsymbol{k})^{1/2} \times \exp(-2\pi i\boldsymbol{r}\cdot\boldsymbol{k}) + \sum_j\left(\sigma_G^2(j)G'_{\rm calc}(j)\sum_{\boldsymbol{k}'}m_{\boldsymbol{k}'}\right)^{-1}\left[G'_{\rm calc}(j) - G_{\rm obs}(j)\right] \times \sum_{\boldsymbol{k}'}m_{\boldsymbol{k}'}F'_{\rm calc}(\boldsymbol{k}')P(\boldsymbol{k}')^{1/2}\exp(-2\pi i\boldsymbol{r}\cdot\boldsymbol{k}')\Bigg]\Bigg\} \tag{6}$$

where

$$G'_{\rm calc}(j) = \left(\sum_{\boldsymbol{k}'}m_{\boldsymbol{k}'} \mid F'_{\rm calc}(\boldsymbol{k}') \mid^2 \Big/ \sum_{\boldsymbol{k}'}m_{\boldsymbol{k}'}\right)^{1/2}. \tag{7}$$

In this work, equation (6) was used for the MEM analysis.

The number of pixels used in the calculation was $60\times60\times60$ for a unit cell, which is fairly large for an MEM analysis. Such a large calculation was efficiently performed without any difficulties by the newly coded MEM analysis program package MEED [23]. This program can be most effectively executed by a supercomputer. In table 1, both the structure factors $F'_{\rm calc}$ calculated considering preferred orientation effects and those $F_{\rm calc}$ calculated purely from the MEM map are also included.

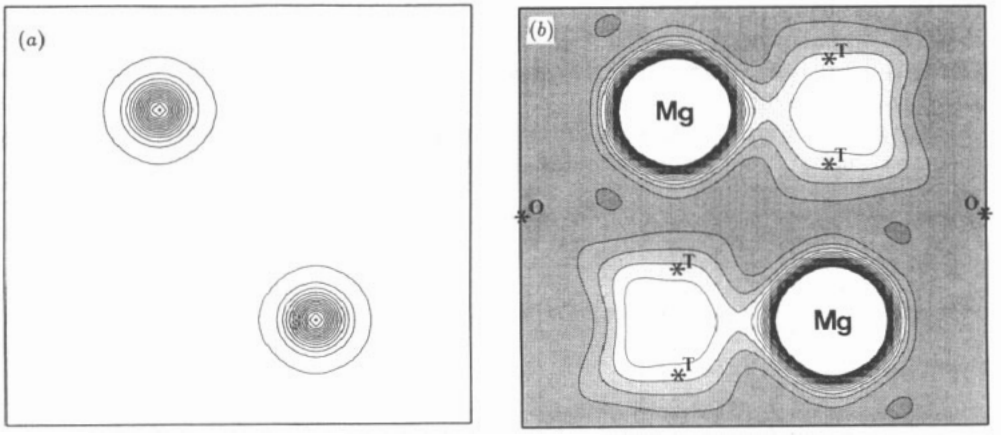

Figure 3. The MEM map of Mg(110) plane (*a*) for the higher-density region (~1.00–71.00 e Å^{-3} with 5.00 e Å^{-3} intervals) and (*b*) for the lower-density region (~0.00–1.00 e Å^{-3} with 0.05 e Å^{-3} intervals).

5. The MEM map of Mg

In figure 3, the MEM map of the Mg(110) plane, which corresponds to two stacking layers, is shown. In figure 3(*a*), the electron densities higher than 1.00 e Å^{-3} are shown. Such higher densities of electrons may be regarded as the density distribution of core electrons. In figure 3(*b*), the densities lower than 1.00 e Å^{-3}, which may be the contribution of the conduction electrons, are shown. The boundary between low and high, i.e. 1.00 e Å^{-3} in the present case, is, of course, tentative. As is well known, there are no negative density

regions in the MEM map. From figure 3(*a*), it is obvious that the core electron density of Mg is quite a spherical feature. This seems to be consistent with the fact that the c/a value of Mg is close to the ideal value. In figure 3(*b*), the distribution of conduction electrons in real space is clearly shown for this substance. It is seen from the figure at first glance that a surplus of electrons can be seen in the bipyramidal space around the tetrahedral sites (T sites; indicated as T in the figure). These surplus electrons are connected to electrons around the atomic sites. On the other hand, electron densities around the octahedral sites (O sites; indicated as O) are very low. This fact may be described as electron deficiencies observed around O sites. It could, therefore, be said that the characteristic features of the spatial distribution of electrons in Mg metal are isotropic distribution of core electrons, surplus electrons around T sites and electron deficiencies around O sites.

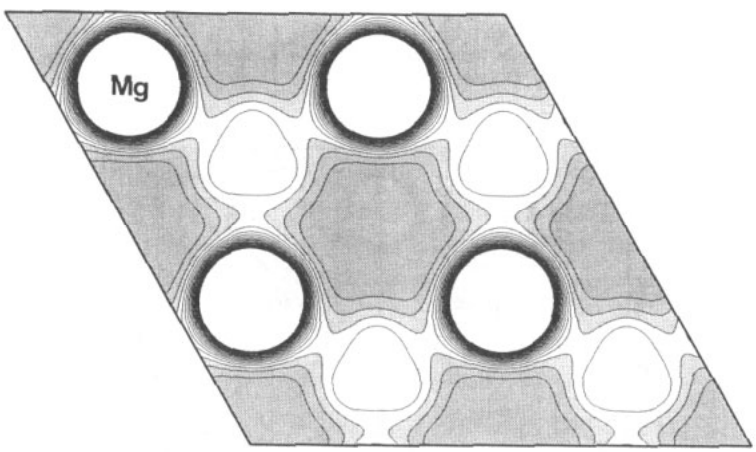

Figure 4. The MEM map of the basal plane for Mg which corresponds to the (001) plane of HCP structure. The electron density region shown in the figure is from 0.00 to 1.00 e $Å^{-3}$ with 0.05 e $Å^{-3}$ intervals. The contour lines for densities of core electrons higher than 1.00 e $Å^{-3}$ are omitted. In order to see the connectivity of electrons, four unit cells are shown in the figure.

In order to reveal the three-dimensional distribution of surplus electron charge, the MEM maps for some other planes are shown. In figure 4, the MEM map of the Mg(001) plane is shown. Since this corresponds to the crystal structure in the basal plane of Mg at the electronic level in real space, it would be of great advantage to examine the nature of chemical bonding in the crystals. It is understood that the surplus electrons around the T sites form a kind of multi-centre bond, i.e. a three-centred bond in the present case, and that they are connecting atoms forming honeycomb network within one stacking layer.

In order to examine the configuration of such a network of surplus electrons further, a new illustration of the electron density distribution is performed, namely the MEM map for the zigzag planes composed of crystallographically equivalent {110} planes. This zigzag plane, which is shown schematically in figure 5, contains both the tetrahedral and the atomic sites. Such an illustration seems to be convenient to study the stacking nature of the honeycomb network as has already been done in the case of Be by Takata *et al* [2]. The zigzag plane of Mg is shown in figure 6. The lower density regions of four stacking layers are shown in the figure. It shows that the honeycomb network actually forms an electronic layer and that there are no significant overlaps between the layers. In other words, it can be said for the structure of Mg at the electronic level that well defined electronic layers are

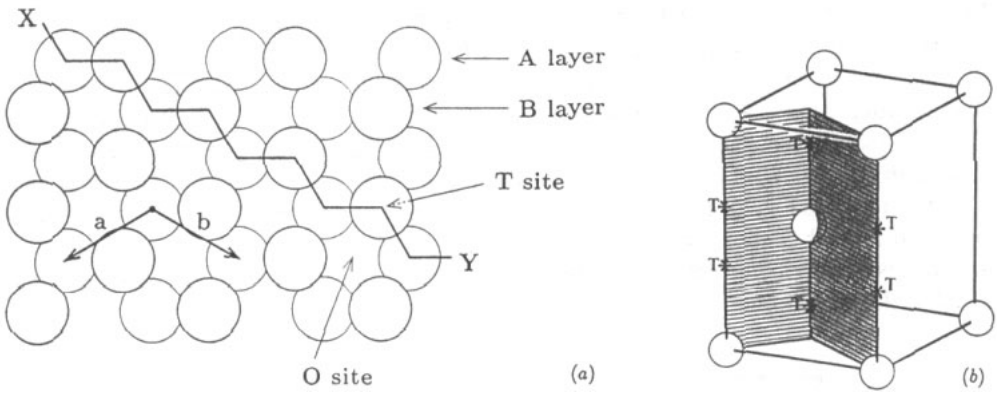

Figure 5. The schematic diagram of zigzag planes for which the MEM map is shown in figure 6. (*a*) is top view, (*b*) side view.

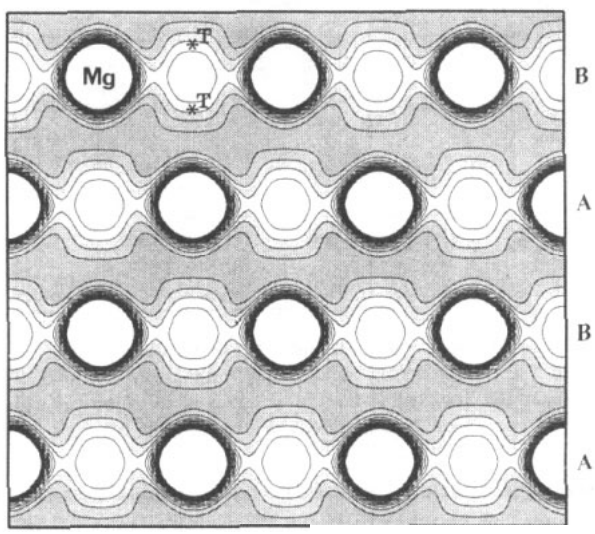

Figure 6. The MEM map of Mg for the zigzag plane shown in figure 5. The contour intervals are the same as in figure 3(*b*).

formed in each stacking layer. As a whole, it could be said that the plane wave description is not suitable for the conduction electrons of HCP metals.

6. Discussion

As is seen in table 1, the difference between F'_{calc} and F_{calc} of Mg is rather small. This means the effects of preferred orientation are not severe. It is still necessary to understand what kind of influence they would cause in the final results, particularly on the electronic layer of Mg. In order to investigate the influence of preferred orientation, the MEM analysis was performed ignoring the preferred orientation effects by using equation (2) instead of equation (6). The MEM map obtained by such an analysis was not significantly different from figures 3, 4 and 6. Only minor differences of the shapes of contour lines were recognized.

Consequently, it is understood that the description in section 5 of the electronic structure of Mg need not be changed at all, even when the preferred orientation effects are ignored.

If there are stacking disorders in the specimen, the present results might be influenced. In order to investigate such a possibility, the FWHMs of $h0\ell$ reflections are carefully examined, since stacking disorders should cause a widening of this type of reflection. However, a significant difference of the FWHM of $h0\ell$ reflections compared with $hh\ell$ reflections, which are the fundamental reflections, was not recognized. It was concluded that the stacking disorders had not significant influence on the present results and that the characteristic features of electronic structures of Mg obtained by this work were intrinsic.

It is, in principle, possible to calculate the total charge of ion cores from the MEM map by counting the number of electrons enclosed in a certain sphere. In order to practice this, the radius of the sphere has to be decided. There are, however, no simple criteria to determine such a radius. In this work we assumed that the radius is half of the distance between the atomic site and the centre of the bipyramidal space of two adjacent tetrahedral holes. By this assumption, the ionic charge of the Mg ion core was calculated as +1.99 and that of Be was +1.71, which is slightly different from the number of valence electrons of Be. A Bader type topological analysis may provide a better way to find the boundary of the Mg core in future works.

It may be interesting to point out the differences of the MEM map of Be and Mg. The electron densities of surplus electrons at the peak position was 0.37 e $Å^{-3}$ for Be and 0.31 e $Å^{-3}$ for Mg, which are almost identical. On the other hand, the electron densities at the O sites were rather different, i.e. 0.25 e $Å^{-3}$ for Be and 0.08 e $Å^{-3}$ for Mg. These differences of the electron density distributions could be related to the structural and physical properties of Mg and Be, i.e. the value of c/a, the high cohesive energy of Be, etc.

As was revealed in this work, the bonding character of even pure metals is not always as simple as the nearly free electron (NFE) model. It would be very interesting to study structures of intermetallic compounds at the electronic level by using the present method. Intermetallic compounds show much variety in physical and chemical properties, which is often considered to have a strong correlation with the crystal and electronic structures. The basic structures of most intermetallic compounds are well known and there would be no difficulty in applying the present method to such compounds.

Acknowledgments

The computations were carried out at the Nagoya University Computer Centre. The authors thank Professor N Sakabe and Drs A Nakagawa and N Watanabe of the Photon Factory for kind help and suggestions for data collection. This work was supported by the Photon Factory, KEK under the proposal No 89-176, and partly by a grant-in-aid from the Ministry of Education, Science and Culture in Japan to which the authors' thanks are due.

Appendix. Notations for MEM equations

$\rho(\boldsymbol{r})$	Electron density at a certain pixel located at $\boldsymbol{r}$.
$\tau(\boldsymbol{r})$	Prior electron density.
$F_{\rm obs}(\boldsymbol{k})$	Observed structure factor for the reflection $\boldsymbol{k}$.
$F_{\rm calc}(\boldsymbol{k})$	Calculated structure factor for the reflection $\boldsymbol{k}$ calculated from $\rho(\boldsymbol{r})$.
$F'_{\rm calc}(\boldsymbol{k})$	Calculated structure factor for the reflection $\boldsymbol{k}$ considering preferred orientation effects.

$\sigma_F(\boldsymbol{k})$	Standard deviation for $F_{\rm obs}(\boldsymbol{k})$.
$G_{\rm obs}(j)$	Observed combined structure factor for jth overlapped peak.
$G_{\rm calc}(j)$	Calculated combined structure factor for jth overlapped peak calculated from $\rho(\boldsymbol{r})$.
$\sigma_G(j)$	Standard deviation for $G_{\rm obs}(j)$.
$G'_{\rm obs}(j)$	Observed combined structure factor considering preferred orientation effects.
$G'_{\rm calc}(j)$	Calculated combined structure factor considering preferred orientation effects.
$\sigma_{G'}(j)$	Standard deviation for $G'_{\rm obs}(j)$.
N_1	Number of independent reflections.
N_2	Number of combined reflections.
V	Unit cell volume.
λ	Lagrange undetermined multiplier.
F_0	$F_{\rm calc}(0)$, which is equal to the total number of electrons in a unit cell.
m_j	Multiplicity for jth overlapped peak.
$P(\boldsymbol{k})$	Preferred orientation factor for the reflection $\boldsymbol{k}$.
$\phi(\boldsymbol{k})$	Acute angle between the preferred orientation direction and the scattering vector $\boldsymbol{k}$.
p	Parameter of preferred orientation correction.

References

[1] Takata M, Yamada M, Kubota Y and Sakata M 1992 *Advances in X-ray Analysis* vol 35 (New York: Plenum) pp 85–90
[2] Takata M, Kubota Y and Sakata M 1993 *Z. Naturf.* a **48** 75–80
[3] Rossmanth E 1984 *Acta Crystallogr.* B **40** 244–9
[4] Merisalo M and Larsen F K 1979 *Acta Crystallogr.* A **35** 325–7
[5] Rossmanth E 1978 *Acta Crystallogr.* A **34** 497–500
[6] Field D W 1982 *Acta Crystallogr.* A **38** 10–2
[7] Brown P J 1972 *Phil. Mag.* **26** 1377–94
[8] Stewart R F 1977 *Acta Crystallogr.* A **33** 33–8
[9] Larsen F K and Hansen N K 1984 *Acta Crystallogr.* B **40** 169–79
[10] Yang Y W and Coppens P 1978 *Acta Crystallogr.* A **34** 61–5
[11] Sakata M and Sato M 1990 *Acta Crystallogr.* A **46** 263–70
[12] Sakata M, Mori R, Kumazawa S, Takata M and Toraya H 1990 *J. Appl. Crystallogr.* **23** 526–34
[13] Sakata M, Uno T, Takata M and Mori R 1992 *Acta Crystallogr.* B **48** 591–8
[14] Sakata M, Takata M, Kubota Y, Uno T and Kumazawa S 1992 *Advances in X-ray Analysis* vol 35 (New York: Plenum) pp 77–83
[15] Sakata M, Takata M, Oshizumi H, Goto A and Hondo T 1992 *Physics and Chemistry of Ice* (New York: Plenum) pp 62–8
[16] Sledziewska-Blocka D and Lebech B 1976 *Acta Crystallogr.* A **32** 150–3
[17] Yukino K and Uno R 1986 *Japan. J. Appl. Phys.* **25** 661–6
[18] Toraya H 1986 *J. Appl. Crystallogr.* **19** 440–7
[19] Will G, Parrish W and Huang T C 1983 *J. Appl. Crystallogr.* **16** 611–22
[20] Collins D M 1982 *Nature* **298** 49–51
[21] Kumazawa S, Takata M and Sakata M 1993 *Acta Crystallogr.* A submitted
[22] Toraya H and Marumo F 1981 *Mineral J.* **10** 211–21
[23] Kumazawa S, Kubota Y, Takata M, Sakata M and Ishibashi Y 1993 *J. Appl. Crystallogr.* **26** 453–7